crystals

MDPI

Article

Characterization and Structural Analysis of Genkwanin, a Natural Product from *Callicarpa americana*

Gina Porras [1,†], John Bacsa [2,†], Huaqiao Tang [1] and Cassandra L. Quave [1,3,4,*]

1 Center for the Study of Human Health, Emory College of Arts and Sciences, Atlanta, GA 30322, USA
2 X-ray Crystallography Center, Emory University, 1515 Dickey Dr, Atlanta, GA 30322, USA
3 Department of Dermatology, Emory University School of Medicine, Atlanta, GA 30322, USA
4 Emory University Herbarium, Atlanta, GA 30322, USA
* Correspondence: cquave@emory.edu
† These authors contribute equally to this work.

Received: 26 July 2019; Accepted: 18 September 2019; Published: 24 September 2019

Abstract: The natural compound Genkwanin (systematic name: 5-hydroxy-2-(4-hydroxyphenyl)-7-methoxychromen-4-one) $C_{16}H_{12}O_5$ (**1**) is a non-glycosylated flavonoid isolated from *Callicarpa americana*. Microcrystals of Genkwanin were prepared by slow evaporation of a methanol solution under low temperature conditions. The structure of **1** was determined based on spectroscopic analyses, one-dimensional NMR, HRESIMS and was confirmed by single-crystal X-ray diffraction. The crystals grow as very thin needles with an extremely high aspect ratio and with the long axis (along the *y*-axis) corresponding to the very short unit cell *b*-axis. There are two independent molecules in the asymmetric unit with two different conformations and modes of packing in the crystal. One molecule has a higher degree on non-planarity than the other. The short stacking distance and separation between the molecules implies a high degree of co-planarity consistent with a conjugated system. The crystal structure is non-centrosymmetric but achiral.

Keywords: Crystal structure; Genkwanin; flavonoid; natural products; *Callicarpa americana*; bioactive substances; anti-bacterial and anti-tumor substances

1. Introduction

The genus *Callicarpa* belongs to the Lamiaceae plant family and contains about 190 species. These species are distributed mainly in tropical and subtropical Asia and Oceanica [1]. Some *Callicarpa* species have been used traditionally as folk medicines for the treatment of coughing, arthritis, bleeding, and abdominal pain [1], suggesting that the genus is a rich source of biologically active natural products. Secondary metabolites from this genus include terpenoids [2–6], lignans [7], glycosides [8] and flavonoids [9], displaying diverse biological effects, such as cytotoxic [2,10], mosquito repellent [5], anti-bacterial [11], antiviral [12], anthelmintic [13] and anti-inflammatory [3] activities.

Callicarpa americana is a shrub native to the south-eastern United States [14]. Preparations of *C. americana* bark have been used to treat fever [15], the leaves to treat dropsy [16], and the roots to alleviate colic [17], dysentery [18], and skin cancer [19]. The roots and branches have been used in preparations intended to relieve malaria, rheumatism, and fever [17] and the leaf essential oils have anti-algal and mosquito-deterrent properties [20].

In our continuous survey on the chemical composition of folk medicines and search for natural bioactive substances, bioassay-guided fractionation resulted in isolation of Genkwanin (**1**), a non-glycosylated flavonoid previously isolated from Genkwa Flos (*Daphne genkwa* Siebold & Zucc.,

Thymelaeaceae) [21], rosemary (*Rosmarinus officinalis* L., Lamiaceae) [22] and the leaves of *Cistus laurifolius* L., Cistaceae [23].

The structure of Genkwanin (**1**) (Figure 1) was first characterized by Wagner et al. [24] and subsequently more fully investigated by various spectroscopic methods [25]. However, this is the first time that the X-ray crystal structure of natural Genkwanin (**1**) is reported. This may be because of the difficulty of growing single crystals that are suitable for single crystal X-ray diffraction.

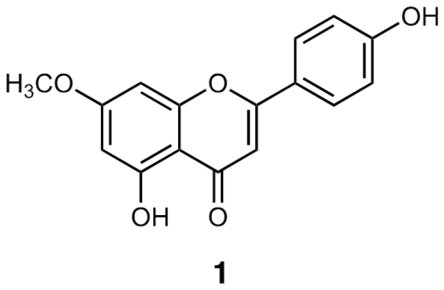

1

Figure 1. The chemical structure of Genkwanin (**1**).

Previous pharmacological studies have found that Genkwanin has a variety of pharmacological effects, including anti-tussive, expectorant, anti-bacterial [26,27], anti-plasmodial [28], free radical scavenging activity [29] and especially anti-inflammatory [30] and anti-cancer properties [31,32].

Mechanistically, flavonoids play a major role by interacting between different types of genes and enzymes. They exert their activity by several mechanisms of action, such as carcinogen inactivation, triggering cell cycle arrest, induction of apoptosis, and inhibition of angiogenesis [33–35]. However, the precise mechanism responsible for the antitumoral effects of these compounds is not yet clearly understood.

The beneficial biological activities of flavonoids are undoubtedly related to their structural composition and attributes, making them ideal lead candidates for the development of pharmaceuticals [36,37]. Understanding the structure–activity relationships of flavonoids like Genkwanin is critical to the development of more potent and effective derivatives for specific targets.

In this study, we provided a detailed description of the molecular structure of Genkwanin. Understanding the three-dimensional structure of this compound will be useful for the study of the interactions between macromolecules (proteins, membrane receptors) and their ligand drugs (e.g., in silico methods) [38,39], confirming or suggesting mechanisms of action or further experiments in order to analyze and predict the biological activity of new pharmacophores.

2. Materials and Methods

2.1. Chemistry

NMR spectra were recorded on a Bruker AVANCE III HD 600 (600 MHz for ^{1}H-NMR, 5-mm CryoProbe) spectrometer (Bruker Biospin GmbH Rheinstetten, Karlsruhe, Germany) in DMSO solvent. Chemical shifts (δ) were reported in ppm using tetramethylsilane (TMS) as the internal standard. HRESIMS data were taken on a Thermo Scientific LTQ-FTMS and processed with Thermo Scientific Xcalibur 2.2 SP1.48 (San Jose, CA, USA). Flash chromatography was carried out using a CombiFlash®Rf+ Lumen (Teledyne ISCO) system with a RediSep Rf Gold silica column. The X-ray analysis was performed using Rigaku XtaLAB Synergy-S diffractometer.

2.2. Plant Material

Fresh leaves were harvested from wild populations of *C. americana* in Atlanta, GA, in June and August 2017. Voucher specimens were deposited at the Emory University Herbarium (GEO) and species identity was confirmed by botanist Tharanga Samarakoon, PhD. Specimens were digitized and

are available for viewing on the SERNEC portal [40]. Plant material was dried in a dehumidification chamber, then ground into a fine powder through a 2-mm mesh with a Thomas Scientific Wiley Mill (Swedesboro, NJ, USA) and stored at room temperature until further processing.

2.3. Extraction, Isolation and Crystallization

Plant material (powdered leaves) was extracted with methanol (ratio of 1:10 *w*/*v*) three times, 72 h each, at room temperature. Filtered extracts were combined and concentrated to give a dark residue (15 g). The crude extract (Extract ID 649, 15.0 g) was suspended in 400 mL methanol-water (1:4) solution and underwent sequential liquid–liquid partitioning with hexane (3 × 500 mL), ethyl acetate (3 × 500 mL) and *n*-butanol (3 × 500 mL). The combined partitions were evaporated to dryness.

The ethyl acetate partition (649C) was the most active partition by antimicrobial bioassays and was subjected to fractionation through flash chromatography. Fractionation was performed using a CombiFlash®Rf+ flash chromatography system (Teledyne ISCO, Lincoln, NE, USA) with a Redi*Sep* Rf Gold®silica column. The dry load column was prepared by binding 649C to Celite 545 at a ratio of 1:4. Flash chromatography was performed using a four-solvent system of hexane, dichloromethane, ethyl acetate and methanol. The separation was monitored at 254 and 280 nm and the resulting fractions were combined to create 32 fractions. Genkwanin (**1**) was obtained from fraction F15 (649C-F15). Single crystals of **1** were prepared by slow evaporation of a methanol solution under low temperature conditions (4 °C) for 12 h.

Analytical data for Genkwanin (**1**). Colourless needles. ^{1}H NMR (600 MHz, DMSO-d_6): δ 12.98 (s, OH-C(5)), 7.98–7.94 (m, H-C(2′, 6′)), 6.95–6.90 (m, H-C(3′, 5′)), 6.85 (s, H-C(3)), 6.78 (d, *J* = 2.3 Hz, H-C(8)), 6.38 (d, *J* = 2.3 Hz, H-C(6)), 3.87 (s, MeO). NSI-FTMS m/z 283.0611 $[M-H]^-$ (calcd for $C_{16}H_{11}O_5$, 283.0606).

2.4. Refinement

A crystal (0.32 × 0.03 × 0.02 mm^3) was selected and mounted with a loop using paratone oil on a XtaLAB Synergy-S diffractometer with a HYPIX detector. X-ray diffraction data were collected using Cu *K*α radiation. The crystal was kept at a constant T = 100 (1) K during the data collection. Initially, the maximum resolution achieved was θ = 44.491° (1.10 Å). A low-resolution structure gave the connectivity and the essential features of the structure. The sample was recrystallized by slow evaporation of a dilute solution in methanol. The larger crystal gave a higher resolution of 0.794 Å (2θ = 147°). Precession Images for the Genkwanin crystal are shown in the SI. Crystal data, data collection and structure refinement details are summarized in Table 1. The structure was solved with the ShelXT [41] structure solution program using the Intrinsic Phasing solution method and by using Olex2 [42] as the graphical interface. The model was refined with version 2018/3 of SHELXL [43] using Least Squares minimization. All non-hydrogen atoms were refined anisotropically. Due to the low-resolution data, rigid bond restraints for the 1,2- and the 1,3 distances were used. However, at the time the manuscript was being written, better crystals were grown for the X-ray analysis and the data was recollected. These restraints were removed from the structural model. The Kohn-Sham molecular orbitals of the asymmetric unit were obtained with Gaussian 16 software [44] and the local and integrated properties of electron density were calculated with the AIMAll suite of programs [45] to investigate the conjugation in the X-ray structure. The Kohn-Sham molecular orbitals were calculated using a b3lyp/SCCF calculation and a TZVP basis set. During the X-ray refinements, similarity and distance restraints were also used. These restraints were relaxed during the later stages of the refinement. Hydrogen atom positions were calculated geometrically and refined using the riding model. The software packages Olex2 [42], TOPOS [46], Crystal Explorer [47] and VESTA [48] were used to create the figures. The crystallographic data has been deposited into the Cambridge Crystallographic Data Centre, 12 Union Road, CB2 1EZ, UK (fax: +44-1223-336033; e-mail: deposit@ccdc.cam.ac.uk) and is available on request, quoting the deposition number CCDC 1944618.

Table 1. Experimental details.

Crystal Data	
Chemical formula	$C_{16}H_{12}O_5$
M_r	284.26
Crystal system, space group	Orthorhombic, $Pna2_1$
Temperature (K)	100
a, b, c (Å)	19.3911 (7), 3.86568 (19), 32.5877 (11)
V (Å^3)	2442.77 (17)
Z	8
Radiation type	Cu $K\alpha$
μ (mm^{-1})	0.97
Crystal size (mm)	0.28 × 0.03 × 0.02
Data collection	
Diffractometer	XtaLAB Synergy, Dualflex, HyPix
Absorption correction	Multi-scan *CrysAlis PRO* 1.171.40.53 (Rigaku Oxford Diffraction, 2019). Empirical absorption correction using spherical harmonics, implemented in SCALE3 ABSPACK scaling algorithm.
T_{min}, T_{max}	0.386, 1.000
No. of measured, independent and observed [$I > 2\sigma(I)$] reflections	16725, 3900, 2676
R_{int}	0.098
(sin $\theta/\lambda)_{max}$ (Å^{-1})	0.622
Refinement	
$R[F^2 > 2\sigma(F^2)]$, $wR(F^2)$, S	0.056, 0.131, 1.06
No. of reflections	3900
No. of parameters	384
No. of restraints	337
H-atom treatment	H-atom parameters constrained
$\Delta\rho_{max}$, $\Delta\rho_{min}$ (e Å^{-3})	0.26, −0.24

Computer programs: CrysAlis PRO 1.171.40.53 (Rigaku OD, 2019), ShelXT [41], SHELXL [43], Olex2 [42].

3. Results and Discussion

The one-dimensional ^{1}H NMR spectra (600 MHz, in DMSO-d_6; see Figure S1 in the supplementary materials) obtained for Genkwanin (**1**) are in accordance with previously published data [49,50].

The single-crystal structure analysis reveals that Genkwanin crystallizes in the orthorhombic space group $Pna2_1$. The crystal structure is characterized by a very short cell edge b = 3.8663 (7) Å and a very long needle axis. The b-axis coincides with the stacking separation between the molecules and this implies a high degree of co-planarity of the substituents with the aromatic rings. There are two Genkwanin molecules in the asymmetric unit (Figure 2). The crystal structure is non-centrosymmetric but achiral. The best fit of the two independent molecules was obtained. A slightly better fit was obtained if an inversion operation was applied to one of the molecules. The 2-phenyl-4*H*-chromen-4-one system shows conjugation between the aromatic ring and the pyran-4-one group and this system adopts a nearly planar conformation. One molecule has a lower planar conformation than the other. The torsion angle between the plane of the p-hydroxyphenyl ring and the pyranone ring is 4.1(2)° in one molecule and 2.3(2)° in the other molecule.

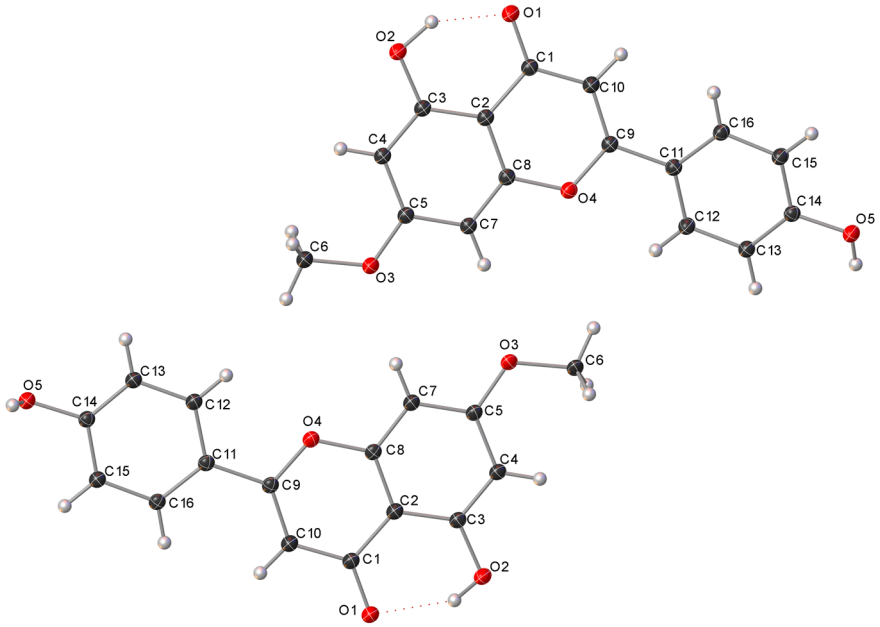

Figure 2. Projections of the two independent Genkwanin molecules (**1a** and **1b**) with their crystallographic numbering.

There appears to be little steric resistance by the Genkwanin molecule's substituents to adopting a planar conformation and the entire molecule adopts a near planar conformation (with some twisting of the phenol substituents). It seemed unlikely that there would be conjugation throughout the entire system and that the planarity provides more efficient packing because the π-stacking is a principal packing force in the crystal. The degree of conjugation was assessed by considering the C-C bond that links the two planar moieties. Its bond distance (1.457(7) Å in molecule 1, 1.452(6) Å in molecule 2) is somewhat shorter than a typical C-C single bond (1.52 Å). There is a useful correlation between the bond orders and their electron delocalization indexes (DI) within a covalently bonded molecule. The delocalization indexes of linked atoms through bond paths are systematically lower than formal bond orders because the valence density is also shared between atoms not connected by formal bonds. The delocalization indexes (and the detailed geometrical parameters) are presented in the supplementary information (Tables S1 to S7). The aromatic rings in Genkwanin have DIs in the range 1.3 to 1.4 (i.e., systematically less than 1.5) and the single bonds have indices between 0.94 and 0.96. The C-C linker has a DI of 1.06. This bond has partial double bond character and there is some delocalization throughout the whole molecule. Interestingly, the calculation also indicates that there is partial keto-enol tautomerization between the C=O and the C-OH group, and that there is a strong pairwise interaction between the two Genkwanin molecules (that extend throughout the crystal). The two unique Genkwanin molecules in the asymmetric unit do not take part in two types of distinct packing. Both are stacked above each other along lines that are parallel to the *b*-axis and with a stacking distance that coincides with the *b*-repeat distance exactly. However, this needs clarification. Although the centroid-to-centroid distance between the stacked Genkwanin molecules is exactly 3.86 Å, the stacking distances between the aromatic moieties are between 3.434 and 3.480 Å and are significantly shorter than the centroid-centroid distance. The Hirshfeld analysis described below shows that the greatest number of contacts occurs at 3.60 Å. The molecules are tilted with respect to each other. The two distinct packing arrangements that were observed are described in further detail. The 2-phenyl-4*H*-chromen-4-one closest to the cell's origin forms an infinite one-dimensional chain held together by strong hydrogen bonds via the phenolic hydrogen O5–H5 and the pyranone oxygen (Figures 3 and 4, Table 2). The second 2-phenyl-4*H*-chromen-4-one forms an almost identical infinite one-dimensional chain held together by hydrogen bonds via the phenolic hydrogen O5–H5 and the pyranone oxygen although the phenolic group is rotated about the rest of the molecule to a greater

extent. The Genkwanin molecules within the chains are not co-planar but corrugated. These infinite one-dimensional chains are parallel with the *a*-axis and perpendicular to the stacking direction (along *b*). Thus, the total structure contains two dimensional planes of Genkwanin molecules (**1a** and **1b**).

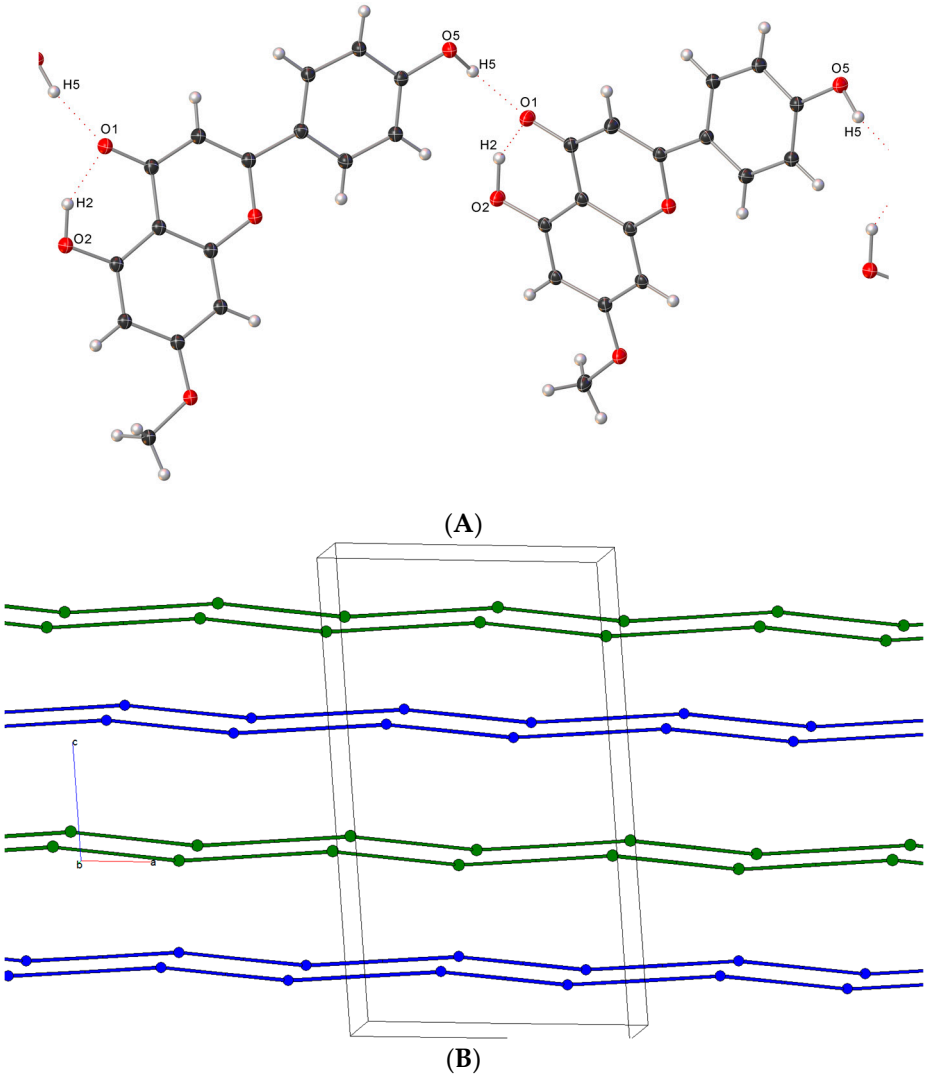

Figure 3. (**A**) A subnet consisting of an infinite, one-dimensional chains of Genkwanin molecules bridged by hydrogen bonds O2–H2···O1_1 (1.76 Å (**a**) and 1.80 Å (**b**)). (**B**) The chains follow the *a*-axis. The simplified nets of the two different Genkwanin molecules form two non-interpenetrating networks (blue (**a**) and green (**b**)). Interestingly, the Genkwanin molecules are more strongly held along chain (**a**) with a slightly shorter separation between the molecules than in **b**.

Table 2. Hydrogen-bond geometry (Å, °).

D—H···*A*	*D*—H	H···*A*	*D*···*A*	*D*—H···*A*
O2_1—H2_1···O1_1	1.00	1.75	2.576 (5)	137.7
O5_1—H5_1···O1_1i	1.00	1.77	2.749 (5)	164.3
O2_2—H2_2···O1_2	1.00	1.72	2.589 (5)	143.6
O5_2—H5_2···O1_2ii	1.00	1.80	2.747 (5)	156.8

Symmetry codes: (i) $x + 1/2, -y + 5/2, z$; (ii) $x - 1/2, -y - 1/2, z$.

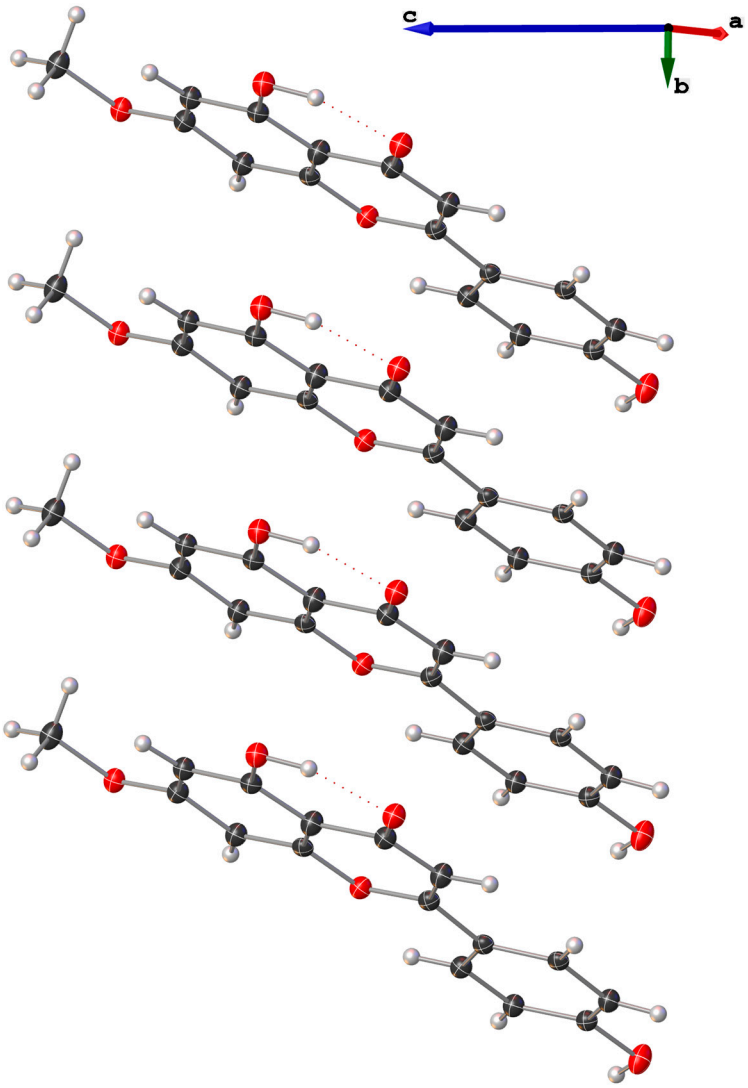

Figure 4. An infinite one-dimensional chain of π-stacked Genkwanin molecules (**1a**) the molecules are tilted but the chain is coincident with the *b*-axis with a separation of (3.8663 (7) Å). The stacking dictates the length of the *b*-axis.

These two directions are dominated by hydrogen bonds and π-stacking but the third direction (along *c*) involves very weak van der Waals forces. The forces in the crystals are strongly directional (strongest along the *b*-axis and weakest along the *c*-direction), resulting in a polar crystal (space group $Pna2_1$) with a strong preference to form needles (Figure 5). Images of the crystal with indexed faces are included in the supplementary data. The crystals grow as very thin needles with an extremely large aspect ratio. The crystals form millimeter long needles but are only 10–20 µm-thick. Photographs of the crystal on the diffractometer are shown in the SI. Although the chains of intermolecular hydrogen bonds follow the *a*-axis, the crystals prefer to grow along the *y*-axis (the needle axis) and this is the direction of the shortest unit cell axis (the *b*-axis). These results seem to indicate that the dominant packing forces that dictate crystal growth are the π-π interactions that follow the *b*-axis and not the hydrogen bonds (along the [010] direction). Although these hydrogen bonds are stronger than π-π interactions, there are many more π-π interactions than hydrogen bonds. We hypothesize that the unusually flat faces of the molecules favor stacking and it is stacking of Genkwanin molecules that is the driving force of the growth of the crystal. However, the condition that π-stacked chains must be connected to each other by hydrogen bonds has to be met form the crystal to form. The inclination

(tilting) seems to indicate that the growth cannot be entirely dictated by the stacking because then the growth would be perpendicular to the planes of the planar rings, which are not coincident to the *b*-axis.

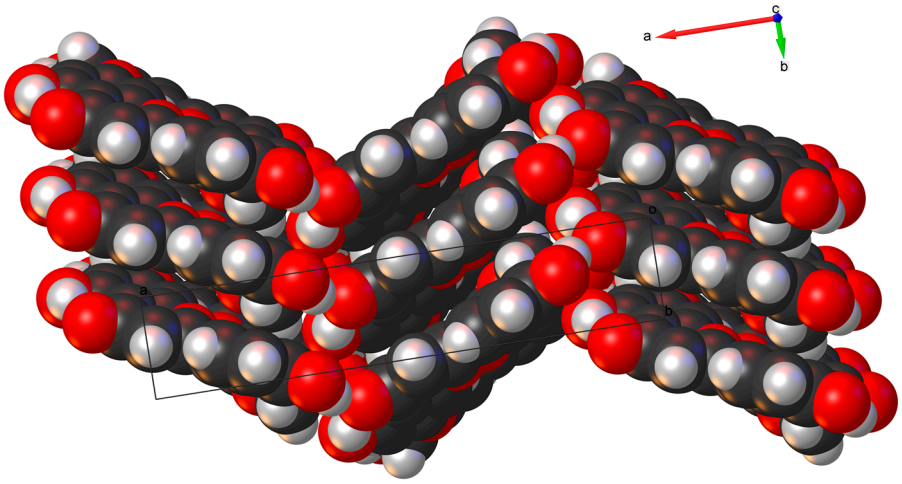

Figure 5. The crystal structure consists of layers that are made up of chains of Genkwanin molecules bridged by hydrogen bonds along the *a*-axis, with adjadcent chains linked by infinite π-π interactions along the *b*-axis. The layers are held together by weaker van der Waals forces along the *c*-axis.

An efficient and straightforward way of describing the striking and complex mix of dissimilar interactions in this crystal is by using Hirshfeld surfaces to partition the crystal space [51]. The Hirshfeld surface for the pair of Genkwanin molecules is shown in Figure 6. The strong hydrogen bond interactions show up as bright red dots. There are large flat regions associated with the π-π interactions and the stacking. There are also some red regions on the flat surfaces, showing that some of the interactions in the flat regions are quite short. These involve the phenolic group, C-H groups and an offset between the stacked molecules along *b*.

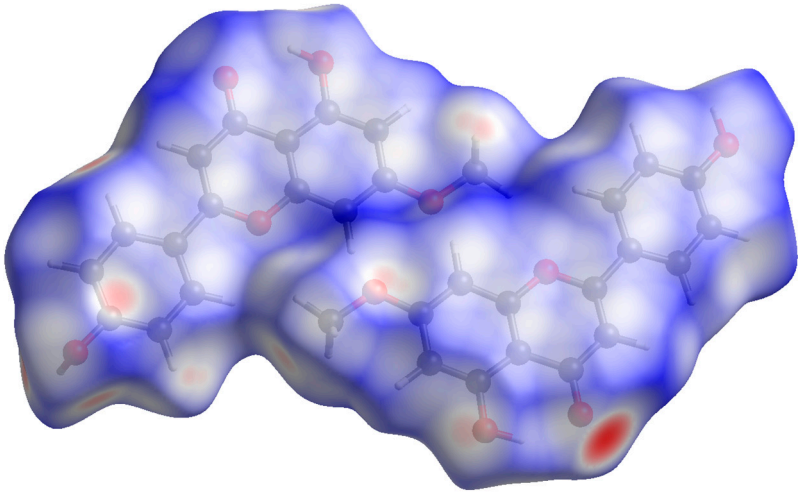

Figure 6. The Hirshfeld surface of the pair of Genkwanin molecules. There are flat depressions on the surface associated with the π-π interactions, dark red spots associated with the hydrogen bonds, and blue regions associated with the weaker van der Waals forces along the *c*-axis, but there are also some short contacts (light red regions) along the stacking region.

The fingerprint plot (Figure 7) summarizes the complex information well. It has a very distinctive appearance. The pair of long arms is from the strong hydrogen bonds. The upper arm corresponds to the hydrogen-bond donor and the lower corresponds to the hydrogen-bond acceptor and the shortest contacts in the crystal structure are the tips of these two spikes. The red orange region at

around 3.60 Å are from the π-π interactions. This distance is shorter than centroid-to-centroid distance between stacked Genkwanin molecules and is the optimal distance at which the highest density of intermolecular contacts between Genkwanin molecules occurs. The large number of contacts with these distances indicates a significant contribution made by π-π stacking to the energy of the crystal. The somewhat broadened point between the two arms at 2 Å is characteristic of H-H interactions.

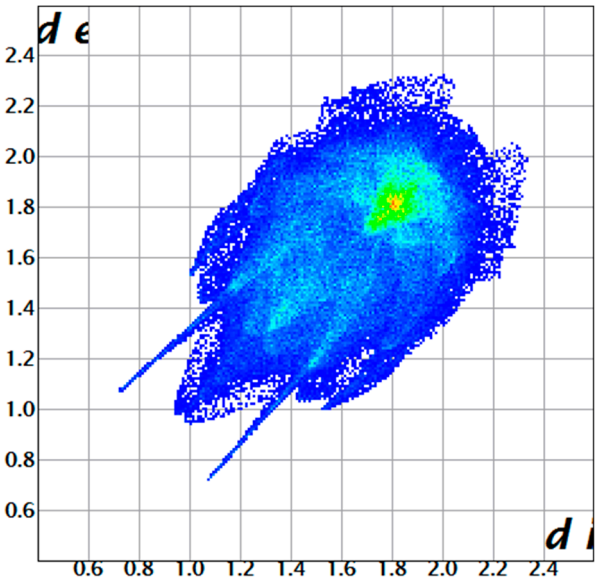

Figure 7. The fingerprint plot of the Genkwanin crystal structure from the Hirshfeld surface. The distinctive features are two spikes from the strong hydrogen bond; a red orange region at around 3.60 Å from the numerous π-π interactions (and a significant contribution from by the π-stacking). The somewhat broadened point between the two arms at 2 Å is characteristic of H-H interactions.

4. Conclusions

During the course of our research into traditional medicine plants, we studied *C. americana* and obtained single crystals of Genkwanin (**1**) by slow evaporation. In this paper, we focused on an in-depth structural characterization of **1** by X-ray crystallography and NMR analyses; this is the first report of the crystal structure of Genkwanin.

The crystal structure of Genkwanin was examined with an emphasis on the conformation of the molecules and the interactions between the molecules in the solid state. The planar arrangement of molecules in projection along the *b*-axis provides efficient packing and the growth direction of the crystals. An examination of the electron density was carried out to assess whether planarity was a result of efficient packing but it was found that there was a small amount conjugation throughout the entire system. These results may indicate a subtle interplay between crystal packing and electronic effects. There are disparate interactions in the crystal and these were found to be highly directional. The crystal morphology was correlated with these packing forces in the crystal. The Hirshfeld analysis and the needle-like morphology indicated that π-π interactions dominate the growth of the crystals. The Hirshfeld surfaces provided a tool for organizing the disparate interactions in the crystal.

Finally, the Genkwanin (**1**) crystal structure could provide novel insights that, together with in silico techniques, improve the understanding of the pharmacological effects of this type of molecule and contribute to the design of new leads that can be rapidly developed into effective treatments to fulfill unmet medical needs.

Supplementary Materials: The following are available online at http://www.mdpi.com/2073-4352/9/10/491/s1, Figure S1. ^{1}H NMR (600 MHz, DMSO-d_6) spectrum of Genkwanin (**1**), Figure S2. Crystal Morphology photos, Figure S3. Precession photographs for Genkwanin crystals, Figure S4. The molecular graph of the asymmetric unit with the bond critical points and the values of the bond delocalization indices (DI's), Table S1. The properties

of the bond critical points between atoms. The bond localization indices (DI) are shown in the last column, Table S2. Crystal data Genkwanin **1**, Table S3. Data collection Genkwanin **1**, Table S4. Refinement, Table S5. Fractional atomic coordinates and isotropic or equivalent isotropic displacement parameters (Å^2) for Genkwanin **1**, Table S6. Atomic displacement parameters (Å^2) for Genkwanin **1**, Table S7. Geometric parameters (Å, °) for Genkwanin **1**.

Author Contributions: G.P., J.B. and C.L.Q. wrote the manuscript. H.T. undertook chemical isolation. G.P. assisted with compound isolation, undertook MS and NMR work and analyzed the chemistry data. J.B. performed the X-ray crystallography experiments and data analysis. All authors contributed to the revision and final review of the manuscript.

Funding: This work was supported by a grant from the National Institutes of Health, National Institute of Allergy and Infectious Diseases (R21 AI136563, PI: C.L.Q.). The content is solely the responsibility of the authors and does not necessarily reflect the official views of NIAID or NIH. The funding agency had no role in study design, data collection and analysis, decision to publish, or preparation of the manuscript.

Acknowledgments: We thank T. Samarakoon for assistance in collecting and authenticating the botanical materials used in this study.

Conflicts of Interest: The authors declare no conflict of interest.

References

1. Chang, Y.S.H.; Ho, Y.L. *The Illustration of Common Medicinal Plants in Taiwan*; Committee on Chinese Medicine and Pharmacy: Taiwan, China, 2004; Volume 3, p. 40.
2. Jones, W.P.; Lobo-Echeverri, T.; Mi, Q.; Chai, H.B.; Soejarto, D.D.; Cordell, G.A.; Swanson, S.M.; Kinghorn, A.D. Cytotoxic constituents from the fruiting branches of *Callicarpa americana* collected in southern Florida. *J. Nat. Prod.* **2007**, *70*, 372–377. [CrossRef] [PubMed]
3. Liu, Y.W.; Cheng, Y.B.; Liaw, C.C.; Chen, C.H.; Guh, J.H.; Hwang, T.L.; Tsai, J.S.; Wang, W.B.; Shen, Y.C. Bioactive diterpenes from *Callicarpa longissima*. *J. Nat. Prod.* **2012**, *75*, 689–693. [CrossRef] [PubMed]
4. Xu, J.; Harrison, L.J.; Vittal, J.J.; Xu, Y.-J.; Goh, S.-H. Four new clerodane diterpenoids from *Callicarpa pentandra*. *J. Nat. Prod.* **2000**, *63*, 1062–1065. [CrossRef] [PubMed]
5. Cantrell, C.L.; Klun, J.A.; Bryson, C.T.; Kobaisy, M.; Duke, S.O. Isolation and identification of mosquito bite deterrent terpenoids from leaves of American (*Callicarpa americana*) and Japanese (*Callicarpa japonica*) beautyberry. *J. Agric. Food Chem.* **2005**, *53*, 5948–5953. [CrossRef] [PubMed]
6. Liu, H.Y.; He, H.P.; Gao, S.; Chen, C.X.; Shen, Y.M.; Hao, X.J. Two new diterpenoids from *Callicarpa pedunculata*. *Helv. Chim. Acta* **2006**, *89*, 1017–1022. [CrossRef]
7. Shao, Y.; Hu, L.H.; Sim, K.Y.; Goh, S.H. Lignanoids and diterpenoids from *Callicarpa furfuraceae*. *Helv. Chim. Acta* **2006**, *89*, 64–72. [CrossRef]
8. Mei, W.L.; Han, Z.; Cui, H.B.; Zhao, Y.X.; Deng, Y.Y.; Dai, H.F. A new cytotoxic iridoid from *Callicarpa nudiflora*. *Nat. Prod. Res.* **2010**, *24*, 899–904. [CrossRef]
9. Hu, Y.M.; Shen, Y.M.; Gu, Q.X.; Zuo, G.Y.; Hao, X.J. Studies on chemical constituents of *Callicarpa pedunculata*. *Chin. Tradit. Herb Drugs* **2001**, *32*, 1063–1065.
10. Jones, W.P.; Kinghorn, A.D. Biologically active natural products of the genus *Callicarpa*. *Curr. Bioact. Compd.* **2008**, *4*, 15–32. [CrossRef]
11. Kim, Y.S.; Shin, D.H. Volatile constituents from the leaves of *Callicarpa japonica* Thunb. and their antibacterial activities. *J. Agric. Food Chem.* **2004**, *52*, 781–787. [CrossRef]
12. Woo, E.R.; Yoon, S.H.; Kwak, J.H.; Kim, H.J.; Park, H. Inhibition of gp 120-CD4 interaction by various plant extracts. *Phytomed. Int. J. Phytother. Phytopharm.* **1997**, *4*, 53–58. [CrossRef]
13. Lee, K.Y.; Jeong, E.J.; Lee, H.S.; Kim, Y.C. Acteoside of *Callicarpa dichotoma* attenuates scopolamine-induced memory impairments. *Biol. Pharm. Bull.* **2006**, *29*, 71–74. [CrossRef] [PubMed]
14. Mabberly, D.J. *The Plant-Book: A Portable Dictionary of the Vascular Plants*; Cambridge University Press: Cambridge, UK, 1997.
15. Crellin, J.K.P. *A Reference Guide to Medicinal Plants: Herbal Medicine Past and Present*; Duke University Press: Durham, NC, USA, 1997; p. 551.
16. Rafinesque, C.S. *Medical Flora or Manual of the Medical Botany of the United States of North America*; University of Glasgow Library: Philadelphia, PA, USA, 1830; p. 276.
17. Moerman, D.E. *American Medical Ethnobotany. A Reference Dictionary*; York, G.P.N., Ed.; Timber Press: Portland, London, UK, 1977; p. 527.

18. Taylor, L.A. *Plants Used as Curatives by Certain Southeastern Tribes*; Botanical Museum, Harvard University: Cambridge, MA, UK, 1940; p. 88.
19. Hartwell, J.L. *Plants Used Against Cancer. A Survey*; Quarterman Publications: Lawrence, MA, USA, 1982; p. 710.
20. Tellez, M.R.; Dayan, F.E.; Schrader, K.K.; Wedge, D.E.; Duke, S.O. Composition and some biological activities of the essential oil of *Callicarpa americana* (L.). *J. Agric. Food Chem.* **2000**, *48*, 3008–3012. [CrossRef] [PubMed]
21. Kai, H.; Koine, T.; Baba, M.; Okuyama, T. Pharmacological effects of *Daphne genkwa* and Chinese medical prescription, "Jyu-So-To". *Yakugaku Zasshi* **2004**, *124*, 349–354. [CrossRef]
22. Altinier, G.; Sosa, S.; Aquino, R.P.; Mencherini, T.; Loggia, R.D.; Tubaro, A. Characterization of topical antiinflammatory compounds in *Rosmarinus officinalis* L. *J. Agric. Food Chem.* **2007**, *55*, 1718–1723. [CrossRef]
23. Sadhu, S.K.; Okuyama, E.; Fujimoto, H.; Ishibashi, M.; Yesilada, E. Prostaglandin inhibitory and antioxidant components of *Cistus laurifolius*, a Turkish medicinal plant. *J. Ethnopharmacol.* **2006**, *108*, 371–378. [CrossRef] [PubMed]
24. Wagner, H.; Chari, V.M.; Sonnenbichler, J. 13C-NMR-Spektren natürlich vorkommender Flavonoide. *Tetrahedron. Lett.* **1976**, *17*, 1799–1802. [CrossRef]
25. Harborne, J.B. *The Flavonoids: Advances in Research Since 1986*; Springer: Berlin/Heidelberg, Germany, 2009; pp. 448–449.
26. Cottigli, F.; Loy, G.; Garau, D.; Floris, C.; Caus, M.; Pompei, R.; Bonsignore, L. Antimicrobial evaluation of coumarins and flavonoids from the stems of *Daphne gnidium* L. *Phytomed. Int. J. Phytother. Phytopharm.* **2001**, *8*, 302–305.
27. Martini, N.D.; Katerere, D.R.; Eloff, J.N. Biological activity of five antibacterial flavonoids from *Combretum erythrophyllum* (Combretaceae). *J. Ethnopharmacol.* **2004**, *93*, 207–212. [CrossRef]
28. Kraft, C.; Jenett-Siems, K.; Siems, K.; Jakupovic, J.; Mavi, S.; Bienzle, U.; Eich, E. In vitro antiplasmodial evaluation of medicinal plants from Zimbabwe. *Phytother. Res. PTR* **2003**, *17*, 123–128. [CrossRef]
29. Kim, A.R.; Zou, Y.N.; Park, T.H.; Shim, K.H.; Kim, M.S.; Kim, N.D.; Kim, J.D.; Bae, S.J.; Choi, J.S.; Chung, H.Y. Active components from *Artemisia iwayomogi* displaying ONOO(-) scavenging activity. *Phytother. Res. PTR* **2004**, *18*, 1–7. [CrossRef] [PubMed]
30. Gao, Y.; Liu, F.; Fang, L.; Cai, R.; Zong, C.; Qi, Y. Genkwanin inhibits proinflammatory mediators mainly through the regulation of miR-101/MKP-1/MAPK pathway in LPS-activated macrophages. *PloS ONE* **2014**, *9*, e96741. [CrossRef] [PubMed]
31. Suh, N.; Luyengi, L.; Fong, H.H.; Kinghorn, A.D.; Pezzuto, J.M. Discovery of natural product chemopreventive agents utilizing HL-60 cell differentiation as a model. *Anticancer Res.* **1995**, *15*, 233–239. [PubMed]
32. Wang, X.; Song, Z.J.; He, X.; Zhang, R.Q.; Zhang, C.F.; Li, F.; Wang, C.Z.; Yuan, C.S. Antitumor and immunomodulatory activity of genkwanin on colorectal cancer in the APC(Min/+) mice. *Int. Immunopharmacol.* **2015**, *29*, 701–707. [CrossRef] [PubMed]
33. Ginwala, R.; Bhavsar, R.; Chigbu, D.I.; Jain, P.; Khan, Z.K. Potential role of flavonoids in treating chronic inflammatory diseases with a special focus on the anti-inflammatory activity of apigenin. *Antioxidants* **2019**, *8*, 35. [CrossRef] [PubMed]
34. Chahar, M.K.; Sharma, N.; Dobhal, M.P.; Joshi, Y.C. Flavonoids: A versatile source of anticancer drugs. *Pharm. Rev.* **2011**, *5*, 1–12.
35. Casagrande, F.; Darbon, J.M. Effects of structurally related flavonoids on cell cycle progression of human melanoma cells: regulation of cyclin-dependent kinases CDK2 and CDK1. *Biochem. Pharm.* **2001**, *61*, 1205–1215. [CrossRef]
36. Koirala, N.; Thuan, N.H.; Ghimire, G.P.; Thang, D.V.; Sohng, J.K. Methylation of flavonoids: Chemical structures, bioactivities, progress and perspectives for biotechnological production. *Enzym. Microb. Technol.* **2016**, *86*, 103–116. [CrossRef]
37. Rengasamy, K.R.R.; Khan, H.; Gowrishankar, S.; Lagoa, R.J.L.; Mahomoodally, F.M.; Khan, Z.; Suroowan, S.; Tewari, D.; Zengin, G.; Hassan, S.T.S.; et al. The role of flavonoids in autoimmune diseases: Therapeutic updates. *Pharm. Ther.* **2019**, *194*, 107–131. [CrossRef]
38. Hurko, O. Target-based drug discovery, genetic diseases, and biologics. *Neurochem. Int.* **2012**, *61*, 892–898. [CrossRef]
39. Berman, H.M.; Westbrook, J.; Feng, Z.; Gilliland, G.; Bhat, T.N.; Weissig, H.; Shindyalov, I.N.; Bourne, P.E. The protein data bank. *Nucleic Acids Res.* **2000**, *28*, 235–242. [CrossRef]

40. SERNEC. Southeast Regional Network of Expertise and Collections. Available online: http://sernecportal.org/portal/ (accessed on 19 September 2019).
41. Sheldrick, G.M. SHELXT—Integrated space-group and crystal-structure determination. *Acta Crystallogr. Sect. A Found. Adv.* **2015**, *71*, 3–8. [CrossRef] [PubMed]
42. Dolomanov, O.V.; Bourhis, L.J.; Gildea, R.J.; Howard, J.A.K.; Puschmann, H. OLEX2: A complete structure solution, refinement and analysis program. *J. Appl. Cryst.* **2009**, *42*, 339–341. [CrossRef]
43. Sheldrick, G.M. Crystal structure refinement with SHELXL. *Acta Cryst. C* **2015**, *71*, 3–8. [CrossRef] [PubMed]
44. *Gaussian 16 Rev. B.01*; Version: Rev. B.01; Gaussian, Inc.: Wallingford, CT, UK, 2016.
45. *TK Gristmill Software: AIMAll*; Version 17.11.14; TAK: Overland Park, KS, USA, 2017.
46. Blatov, V.A.; Shevchenko, A.P.; Proserpio, D.M. Applied topological analysis of crystal structures with the program package ToposPro. *Cryst. Growth Des.* **2014**, *14*, 3576–3586. [CrossRef]
47. *CrystalExplorer 17*; Version 17; University of Western Australia: Crawley, AU, Australia, 2017.
48. Momma, K.; Izumi, F. VESTA 3 for three-dimensional visualization of crystal, volumetric and morphology data. *J. Appl. Cryst.* **2011**, *44*, 1272–1276. [CrossRef]
49. Kiyekbayeva, L.; Mohamed, N.M.; Yerkebulan, O.; Mohamed, E.I.; Ubaidilla, D.; Nursulu, A.; Assem, M.; Srivedavyasasri, R.; Ross, S.A. Phytochemical constituents and antioxidant activity of *Echinops albicaulis*. *Nat. Prod. Res.* **2018**, *32*, 1203–1207. [CrossRef] [PubMed]
50. Baek, S.C.; Park, M.H.; Ryu, H.W.; Lee, J.P.; Kang, M.G.; Park, D.; Park, C.M.; Oh, S.R.; Kim, H. Rhamnocitrin isolated from *Prunus padus* var. *seoulensis*: A potent and selective reversible inhibitor of human monoamine oxidase A. *Bioorg. Chem.* **2019**, *83*, 317–325. [CrossRef] [PubMed]
51. McKinnon, J.J.; Spackman, M.A.; Mitchell, A.S. Novel tools for visualizing and exploring intermolecular interactions in molecular crystals. *Acta Cryst. B* **2004**, *60*, 627–668. [CrossRef]